REVIEW ARTICLE
https://doi.org/10.1038/s41929-018-0078-5

nature catalysis

Recent trends and fundamental insights in the methanol-to-hydrocarbons process

Irina Yarulina[1,3], Abhishek Dutta Chowdhury[2,3], Florian Meirer[2], Bert M. Weckhuysen[2*] and Jorge Gascon[1*]

The production of high-demand chemical commodities such as ethylene and propylene (methanol-to-olefins), hydrocarbons (methanol-to-hydrocarbons), gasoline (methanol-to-gasoline) and aromatics (methanol-to-aromatics) from methanol—obtainable from alternative feedstocks, such as carbon dioxide, biomass, waste or natural gas through the intermediate formation of synthesis gas—has been central to research in both academia and industry. Although discovered in the late 1970s, this catalytic technology has only been industrially implemented over the past decade, with a number of large commercial plants already operating in Asia. However, as is the case for other technologies, industrial maturity is not synonymous with full understanding. For this reason, research is still intense and a number of important discoveries have been reported over the last few years. In this review, we summarize the most recent advances in mechanistic understanding—including direct C–C bond formation during the induction period and the promotional effect of zeolite topology and acidity on the alkene cycle—and correlate these insights to practical aspects in terms of catalyst design and engineering.

In 1977, scientists at Mobile published the first patent on the methanol-to-hydrocarbons (MTH) process[1], claiming that "A lower alcohol and/or ether feed is selectively converted to a mixture of light olefins, including ethylene and propylene, by catalytic contact of the feed, for example methanol or dimethyl ether, at sub-atmospheric partial pressure, with certain crystalline aluminosilicate zeolite catalysts exemplified by ZSM-5" (Fig. 1a). The possibility to obtain olefins (methanol-to-olefins, MTO or DMTO if the feedstock is dimethylether), aromatics (methanol-to-aromatics, MTA) and/or gasoline (methanol-to-gasoline, MTG) without relying on oil (methanol can be produced from a wide range of carbon-containing sources, such as biomass, waste, coal, natural gas or even carbon dioxide) makes this family of processes a convenient alternative to the classical production routes of high-demand chemicals and intermediates.

As it is the case for other established methods of the petrochemical industry, such as fluid catalytic cracking (FCC)[2], the MTH process — despite being already commercialized — still attracts a great deal of attention from both industry and academia. Apart from the obvious economic driving force in improving the process, from a scientific point of view, understanding (and eventually controlling) the complex reaction mechanism behind such a complex overall stoichiometry remains a challenge. As we will elaborate below, the process is dictated by a large set of elementary reactions and the full picture of the MTH reaction mechanism is still elusive (Fig. 1b). On one hand, the chosen reaction conditions are important, as not all reactions have the same kinetic order and energies of activation; on the other hand, the zeolite microenvironment plays an even bigger role in defining product distribution and catalyst lifetime[3]. MTH therefore serves as an outstanding example of complexity in zeolite chemistry and heterogeneous catalysis, as pinpointed in a number of classical[4] and more recent reviews[5–9].

In this Review, we highlight current challenges of MTH chemistry by critically analysing the existing literature to give an updated picture on the mechanism of reaction and to provide guidelines for catalyst design. We believe that, despite a number of excellent reviews in this field, knowledge on mechanistic aspects and structure–property relationships in MTH has advanced tremendously over the last few years and we expect this Review to bridge the gap between those earlier reviews dedicated to mechanism rationalization and catalyst engineering. To do so, we first summarize the recent efforts to unravel the mechanism that leads to the formation of the first C–C bond (that is, the coupling of two methanol or dimethyl ether molecules), a topic of intense debate over the last few decades. Formation of the direct C–C bond continues with the formation of longer hydrocarbons inside the zeolite pores, this mechanism along with the most recent spectroscopic evidences of its different steps are discussed in the second section. Finally, with this mechanistic information in hand, we define a number of catalyst design rules that should help the reader understand the effect of catalyst topology, acidity and reaction conditions on product distribution and catalyst deactivation. The Review is completed with our personal view on future challenges both from the process and fundamental point of view.

The direct C–C bond

The MTH process involves a very complex reaction mechanism[5–8,10]. As of now, more than 20 different proposals have been postulated in the literature[4]. Surprisingly, the exact route for the formation of the first carbon–carbon (C–C) bond during MTH was only very recently unveiled[11–18]. For a long time, the scientific community assumed that the presence of traces of impurities (for example, in the methanol, catalyst and/or carrier gas) was responsible for the formation of the direct C–C bond over any direct mechanism (that is, the coupling of two methanol molecules). This assumption was primarily attributed to the lack of concrete experimental evidence in support of the direct mechanism[19,20]. Moreover, the feasibility of such direct coupling was anticipated to be low by theoreticians

[1]King Abdullah University of Science and Technology, KAUST Catalysis Center, Advanced Catalytic Materials, Thuwal, Saudi Arabia. [2]Inorganic Chemistry and Catalysis, Debye Institute for Nanomaterials Science, Utrecht University, Utrecht, The Netherlands. [3]These authors contributed equally: Irina Yarulina, Abhishek Dutta Chowdhury. *e-mail: b.m.weckhuysen@uu.nl; jorge.gascon@kaust.edu.sa

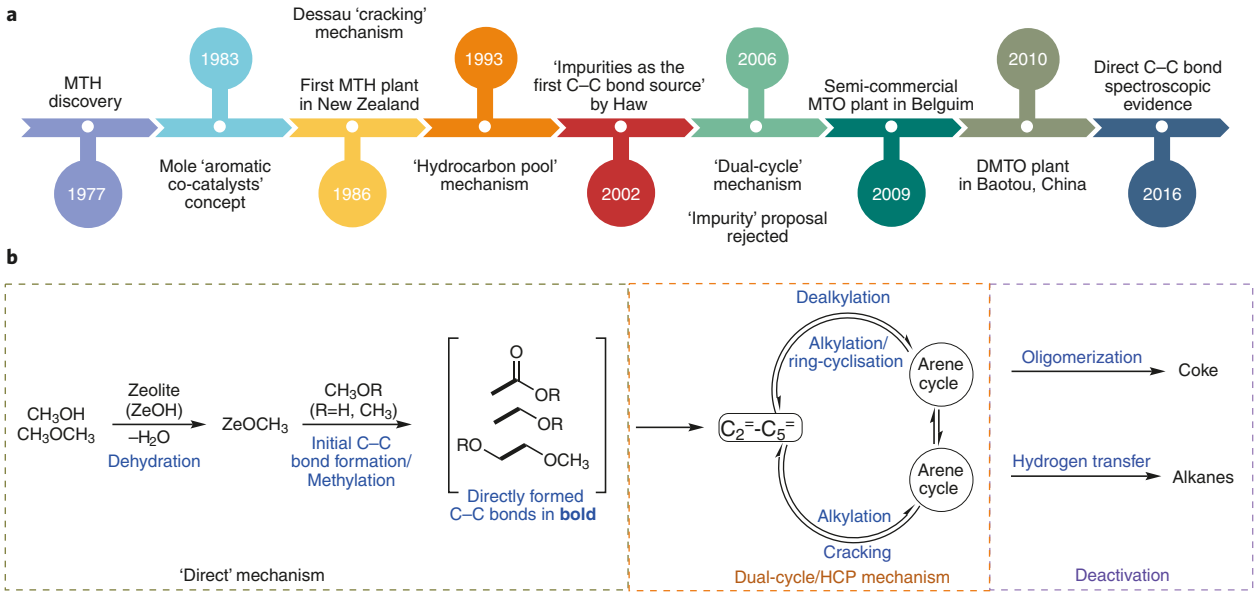

Fig. 1 | Milestones and mechanism development of the MTH process. a, MTH chronology shows that 40 years of combined efforts produced several mechanistic concepts for both the initial induction and steady state periods. The current simplified mechanistic picture is shown in **b**. The simplified scheme of the MTH mechanism reveals that although the aromatic cycle leads to the formation of light olefins, it also acts as a scaffold for coke formation; thus, olefins formation is preferred over the olefins cycle (MTH, methanol-to-hydrocarbons; MTO, methanol-to-olefin; DMTO, dimethylether-to-olefin; ZeOH, zeolite acid sites).

because of the high activation energies and unstable reaction intermediates[21,22]. In 2006, Hunger and co-workers[23] systematically demonstrated that traces of organic impurities neither have any significant influence on product distribution, nor do they control the formation of hydrocarbon pool (HCP, *vide infra*) species during the MTH reaction (Fig. 1a). That means a direct mechanism may be operative, at least in the early stages of the MTH reaction[16]. Since then, research groups (for example, Kondo, Fan, Copéret, Lercher, Weckhuysen and Liu) have delivered both experimental and theoretical evidence in support of the existence of a direct mechanism during the initial stages of MTH[11–18,23–30]. In essence, this reaction can be sub-divided into two parts: direct mechanism and the conventional HCP/dual-cycle mechanism, during the induction and autocatalytic periods, respectively.

There are several excellent reviews available in the literature on this topic that adequately describe the history and developments of direct mechanisms[4,6]. Although a consensus has currently been reached regarding the existence of the direct mechanism, its actual nature/course of action is yet to be fully established. In all direct mechanistic proposals, a surface methoxy species (SMS), formed upon adsorption of methanol onto a Brønsted acid site, is indisputably the most experimentally verified intermediate (Fig. 2)[13,14,18,26]. The ability of the SMS to form a C–C bond at higher reaction temperatures is a well-established phenomenon during any zeolite-catalysed hydrocarbon conversion process[18]. The idea of a carbene-insertion mechanism by the SMS was first introduced by Hunger and colleagues[18,26,27], and was mostly based on NMR spectroscopy and carbene-trapping experiments. The carbene character of the SMS was proposed to form through the polarization of the C–H bond of the SMS by a neighboring adjacent oxygen (as depicted in Fig. 2a–c)[31,32]. The carbene/ylide nature of the SMS was confirmed by a carbene trapping experiment with cyclohexane acting as a probe molecule at ≥493 K, where methylcyclohexane was formed through an insertion reaction of a carbene/ylide into the sp^3 C–H bond of cyclohexane (Fig. 2a)[18]. Later, Kondo and colleagues[11,12] also arrived to the same conclusion with the help of IR spectroscopy: the C–C bond containing hydrocarbon species originated from the coupling between the carbene-like SMS and methanol/dimethyl ether (DME) (Fig. 2b). Another convincing evidence in support of the existence of a carbene-type mechanism was provided recently by Weckhuysen et al.[13], by employing 2D magic-angle spinning (MAS) solid-state NMR (both ^{1}H–^{13}C and ^{13}C–^{13}C) spectroscopy (Fig. 2c). The strong signals at 52.2 (^{13}C) and 3.59 (^{1}H) ppm were assigned to surface adsorbed methanol, whereas the signals at 57.7 (^{13}C) and 3.54 (^{1}H) ppm were attributed to the SMS (red strip in Fig. 3a). Interestingly, a strong cross-peak between these ^{13}C signals was also observed, which was due to the close proximity of surface adsorbed methanol and the SMS (blue strip in Fig. 3a and schematic illustrated in Fig. 2c). Such close proximity does not only reveal the ongoing reaction between SMS and methanol (through the polarization of the C–H bond of the SMS by a neighboring adjacent oxygen atom), but also showcases the carbene/ylide-character of SMS.

Apart from the carbene mechanism, multiple analogues of oxonium and methane–formaldehyde-type direct mechanistic proposals have also been shown in the recent literature. The conventional methane–formaldehyde mechanism of the MTH reaction was originally postulated by Hutchings and colleagues[33] in 1987. The direct C–C bond coupling reaction between methane and formaldehyde, as a result of disproportionation of methanol (through its hydride abstraction by the SMS, as illustrated in Fig. 2d), was hypothesized to pose an unrealistically high energy barrier[22]. However, several recently postulated proposals are conceptually similar to this mechanism. The methoxymethyl cation mechanism proposed by Fan et al.[28,29] was developed from the original proposal of Hutchings and colleagues, in order to make it energetically feasible. Their experimentally and theoretically verified proposal involves the formation of direct C–C bond via: (i) a methoxymethyl cation ($CH_3OCH_2^+$ from SMS and DME, that is, instead of direct formation of formaldehyde), and (ii) its subsequent direct C–C coupling with another DME/methanol molecule to form $CH_3OCH_2CH_2OR$ (R = H, CH_3) (a precursor for olefins, as shown in Fig. 2e)[28,29]. Similarly, the methyleneoxy mechanism was recently reported by Liu and co-workers[14]; based on in situ solid-state NMR spectroscopy by measuring

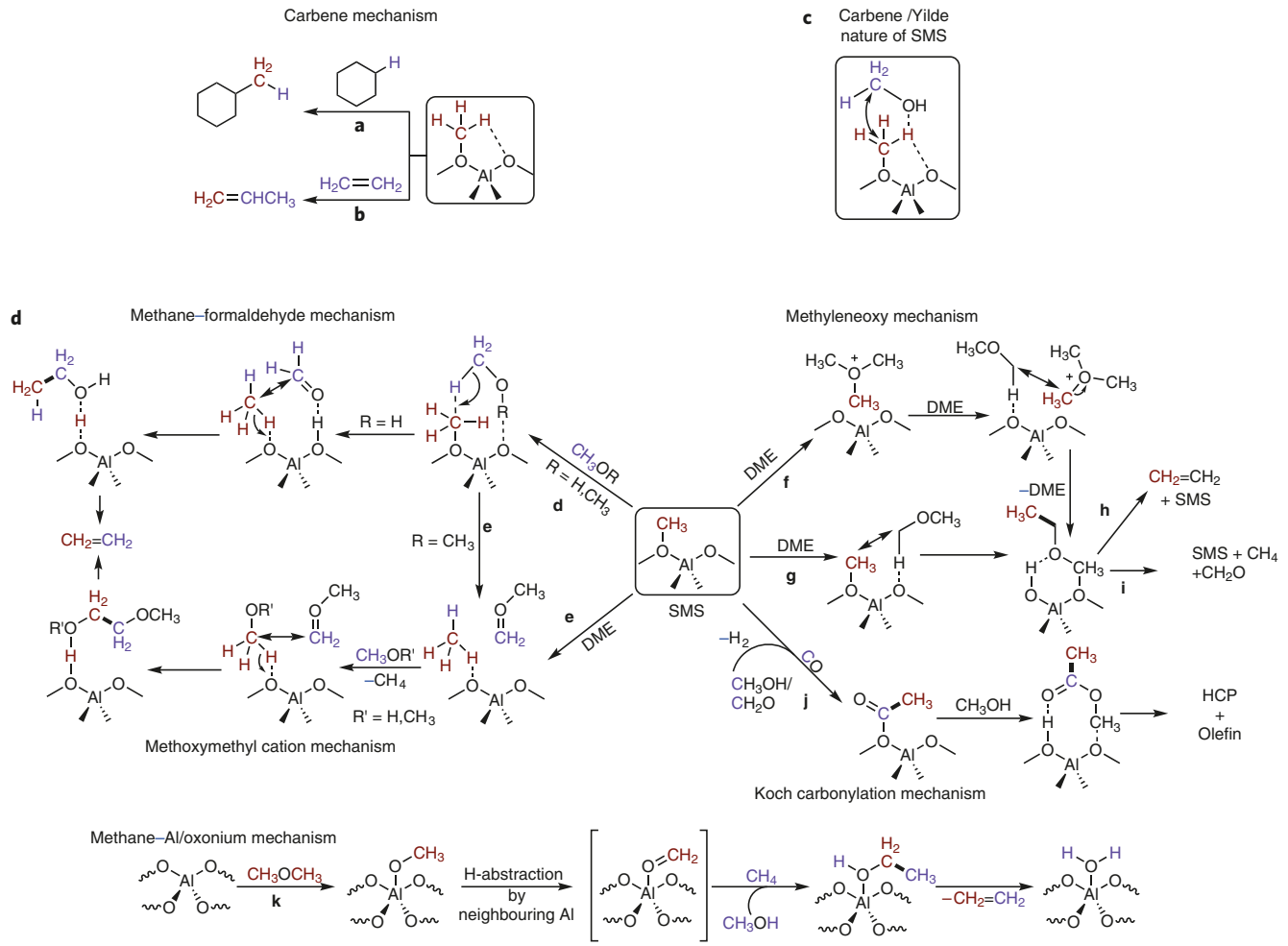

Fig. 2 | Several proposed direct mechanistic routes during the early stages of the zeolite-catalysed MTH process. a,**b**, The proposed mechanism of the methanol conversion reaction between the SMS and cyclohexane (**a**) and ethylene (**b**) via the carbene-type intermediate. **c**, The spectroscopically verified intermediate consists of SMS and methanol, suggesting a possibility of C–H insertion of methanol by carbene-like SMS species. **d**,**e**, Schematic illustration of the conventional methane–formaldehyde mechanism (**d**), and its modified analogue the methoxymethyl cation mechanism (**e**). **f**–**i**, The methyleneoxy mechanism of the MTH reaction, involving either the trimethyloxonium (**f**) or SMS (**g**) intermediate. The SMS involving route initiates the formation of both ethylene (**h**) and methane/formaldehyde (**i**) simultaneously. **j**, Plausible routes for the direct formation of the carbon–carbon bond during early stages of the MTH reaction through Koch-type carbonylation of SMS. **k**, The methane–aluminium/oxonium mechanism for the conversion of methanol over alumina.Credit: panel **a** adapted from ref. [18], American Chemical Society; panels **b** and **c** adapted from refs [11,13], Wiley, respectively; panels **d** and **e** reproduced from refs [29,33], Royal Society of Chemistry; panels **f**–**i** reproduced from ref. [14], Wiley; panel **j** adapted from ref. [13], Wiley; panel **k** adapted from ref. [17], American Chemical Society.

^{13}C-methanol conversion over H-ZSM-5 using a rotor reactor (Fig. 2f,g & Fig. 3b). Three major bands at 59.5, 69.0 and 80.0 ppm were generated almost instantaneously and were assigned to the SMS, surface-adsorbed DME and trimethyl oxonium (TMO), respectively. The appearance of these three bands was accompanied by formation of ethylene (detected by GC-MS) as well as higher hydrocarbons (chemical shifts of δ = 20–40 ppm). Therefore, the direct C–C bond was proposed to be formed as a result of direct interaction between the reactant (methanol/DME) and zeolite-bound surface intermediates: the SMS and TMO (Fig. 2f,g). The important C–H bond-activation step could be assisted by framework oxygen to form active methyleneoxy species (R–O–CH_2–H···zeolite), which eventually leads to the simultaneous formation of both an olefin (Fig. 2h) and methane/formaldehyde (Fig. 2i). The unprecedented downfield response and relatively broader nature of the SMS at 69.0 ppm under in situ reaction conditions (compared to δ = 59.0 ppm under ex situ reaction conditions) was attributed to the strong interaction between the activated DME species and active surface–zeolite catalyst (Fig. 2f,g). Although both methane and formaldehyde are proposed to be involved in the catalytic cycle (by assisting the regeneration of SMS), their role towards the formation of the direct C–C bond was not clarified[14].

Although numerous mechanistic reports have identified formaldehyde as a side-product, its fate/role during the MTH reaction is still a subject of debate. Formation of formaldehyde on solid acid catalysts from methanol is quite predictable, particularly at high temperatures. Interestingly, it could be easily associated to the Koch carbonylation mechanism of the MTH reaction (Fig. 2j), another direct mechanistic route proposed independently by the groups of Lercher and Weckhuysen[13,16] at the same time. Lercher and co-workers[16] first proposed methyl acetate ($CH_3CO_2CH_3$, derived via carbonylation of methanol/DME) as the very first C–C bond-containing intermediate during the MTH reaction over H-ZSM-5. Spectroscopic evidence for this proposal came from the Weckhuysen group[13], whom employed a combination of solid-state NMR spectroscopy (coupled with *operando* UV-visible diffuse

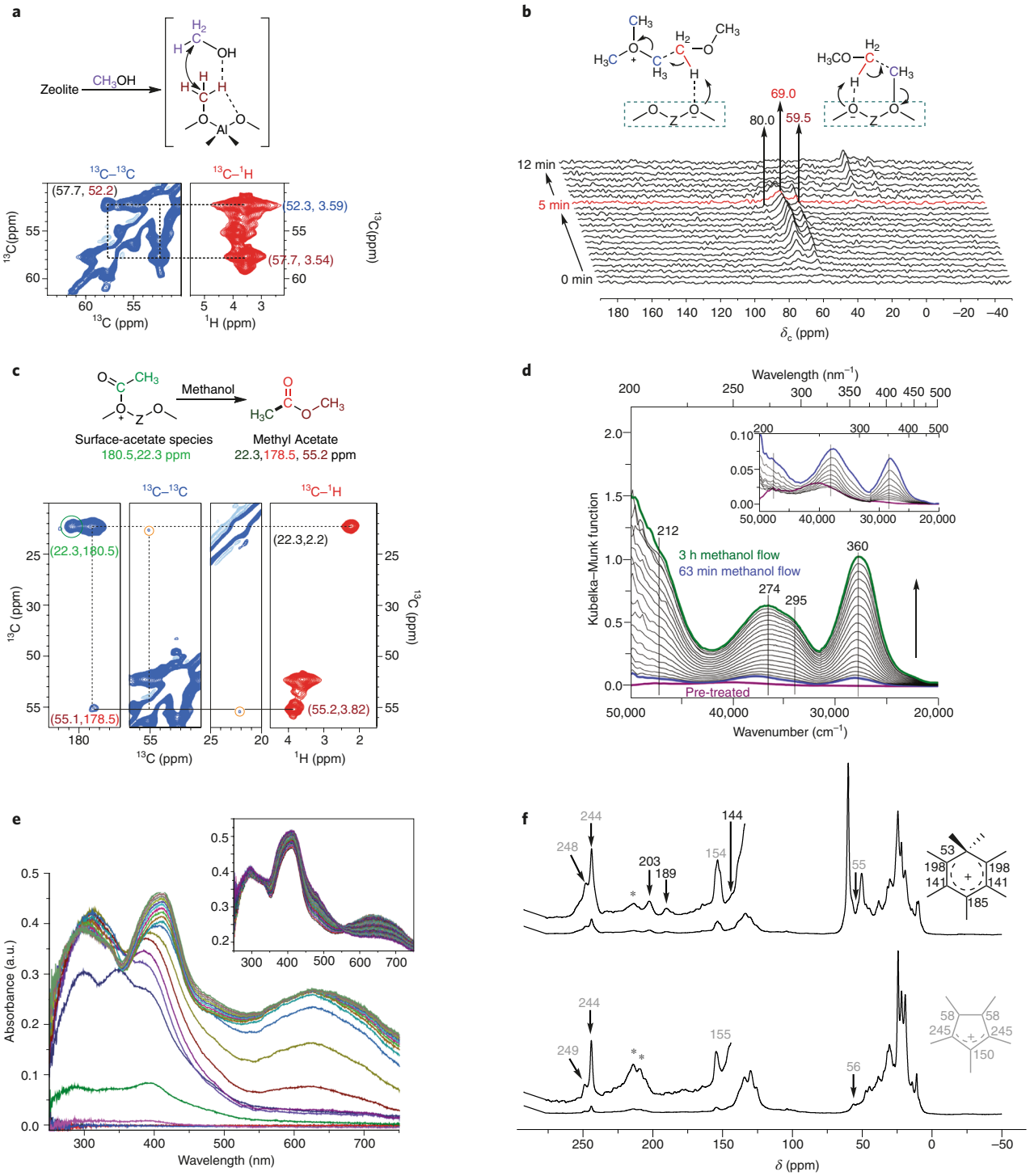

Fig. 3 | The spectroscopic signatures of crucial intermediates during the zeolite catalysed methanol-to-hydrocarbon (MTH) process. a, Solid-state NMR spectra of methoxy in H-SAPO-34 after the MTH reaction for 30 minutes at 673 K. Zooms from 2D ^{13}C–^{13}C (blue strip) and ^{13}C–^{1}H (red strip) magic angle spinning (MAS) solid-state NMR spectra with long mixing (150 ms) and cross-polarization (CP) contact time (500 ms), respectively, identifying surface adduct between SMS and methanol (the arrow in the molecular structure indicates ^{13}C–^{13}C correlation). **b**, In situ ^{13}C MAS solid-state NMR spectra measured during MTH reaction over H-ZSM-5 at 573 K for 12 min. **c**, Solid-state NMR spectra of acetate species in H-SAPO-34 after the MTH reaction for 30 minutes at 673 K. Zooms from 2D ^{13}C–^{13}C (blue strip) and ^{13}C–^{1}H (red strip) MAS solid-state NMR spectra with long mixing (150 ms) or CP contact time (500 ms), respectively, indicating surface acetate and methyl acetate resonances. **d**,**e**, UV-visible diffuse reflectance spectra of H-ZSM-5 (**d**) and H-SAPO-34 (**e**) being exposed to the MTH reaction under in situ (573K) and *operando* (673K) reaction conditions, respectively. An absorption band at 295 nm (**d**) on H-ZSM-5 and 387 nm (**e**) on H-SAPO-34 were assigned to a methylated cyclopentadienium and hexamethylbenzenium ions, respectively. **f**, ^{13}C MAS solid-state NMR spectra of retained organic species in H-SAPO-34 (upper spectrum, 573K, 15 min) and H-SSZ-13 (lower spectrum, 548K, 25 min) after continuous-flow of $^{13}CH_3OH$ for 15 min (asterisks represent spinning side bands, chemical shifts on the molecular structures were theoretically calculated values).Credit: panels **a**–**c** from refs [13,14] and [13], Wiley, respectively; panel **d** reproduced from ref. [46], American Chemical Society; panel **e** reproduced from ref. [13], Wiley; panel **f** reproduced from ref. [53], Wiley

reflectance spectroscopy (DRS) and online mass spectrometry); it was shown that the Koch-carbonylation route occurred during the MTH over H-SAPO-34. In this case, the direct C–C bond containing zeolite-bound acetate species (Fig. 2j) is a Koch carbonylation product of the SMS. Here, either methanol or formaldehyde, in principle, could act as a carbonylating agent under MTH reaction conditions. Next, methyl acetate was formed after methoxylation of surface-bound acetate species, which independently could initiate the formation of HCP species and thus, olefins. In the carbonyl region of the NMR spectrum, clear cross-peaks to methyl carbon atoms were observed at both long and short mixing times (Fig. 3c). The signal at 180.5 ppm shows only one cross-peak — corresponding to a zeolite–acetate species — at 22.5 ppm (Fig. 3c). Moreover, the signal at 178.5 ppm has a clear cross-peak with a ^{13}C signal at 55.1 ppm at longer mixing times only (that is, the methoxy carbon is not directly attached to the carbonyl carbon). This ^{13}C-methoxy signal correlates with a H signal at 3.82 ppm and has an additional very weak correlation signal with a methyl at 22.3 ppm (^{13}C) at longer C–C mixing times (Fig. 3c). This cross-peak pattern is a signature response from a methyl acetate molecule. Thus, all three responsible intermediates of this mechanism (SMS, zeolite-acetate and methyl acetate) were spectroscopically identified by solid-state NMR spectroscopy. This Koch carbonylation mechanism of the MTH reaction has recently been theoretically verified by Plessow and Studt[30]. Interestingly, the simultaneous existence of (at least) two different direct C–C bond-forming routes (that is, carbene and Koch carbonylation) were spectroscopically identified (Fig. 2c,j & Fig. 3a,c).

Another interesting recent report by Copéret et al.[17] should be mentioned: the formation of the direct C–C bond from DME alternatively proposed to be catalysed by extra-framework aluminium atoms in acidic zeolites (Fig. 2k). Herein, the C–C bond forming step initially involves generation of a transient aluminium–oxonium species (that is, formaldehydic oxygen coordinated to a Lewis acidic aluminium) through hydrogen abstraction from an aluminium–methoxy species. Next, aluminium–oxonium species react with a methane molecule to yield the direct C–C bond containing surface–ethanolic species (that is, a precursor for ethylene). This contribution inevitably sparks the controversy about the actual involvement of the zeolitic Lewis acid sites during the direct mechanism of the MTH reaction[15,17]. However, such discussion is beyond the scope of the current review and demands further research to understand the phenomenon at the molecular level.

Dual-cycle concept

After a rather short induction period assigned to the formation of the direct C–C bond, the MTH process continues with the steady-state formation of hydrocarbons in the so-called autocatalytic dual-cycle concept[34]. This notation is the result of merging the two mechanistic schemes developed in parallel for ZSM-5 and SAPO-34[5]. For cage-like zeolites (SAPO-34), able to accommodate large aromatics, light olefins are believed to form via an indirect way through HCP species (Fig. 4). They can be visualized as typical ship-in-a-bottle molecules that can be formed in zeolites but cannot desorb. These species are methylated yielding light olefins such as ethylene and propylene by elimination reactions, thus restoring the initial HCP species. For ZSM-5 and its analogues, formation of hydrocarbons was rationalized as a result of consecutive methylation and cracking reactions already in the 1980s by Dessau[35]. The dual cycle represents a compromise between both mechanisms (olefinic and aromatic cycles) running in parallel (Fig. 4). Both cycles can be subcategorized further to elementary steps described by six types of reactions: methylation and cracking of olefins, methylation and dealkylation of aromatics, hydrogen transfer and cyclization, the latter two acting as the bridging step between the two cycles[8]. Using transient switching experiments $^{12}C/^{13}C$ Svelle et al.[36] showed that, for ZSM-5, all olefins except ethylene are produced from the olefinic cycle. Ethylene evolution was linked to the presence of lower methylbenzenes, suggesting that ethylene is mostly a product of the aromatic cycle[37]. Sun and co-workers[38] further contributed to this topic by performing seminal kinetic investigations at different conversion levels in the presence of aromatic and olefinic co-feeds. They concluded that both cycles are active for ethylene and propylene production, with the aromatic cycle giving similar selectivity for both olefins. The olefinic cycle, on the other hand, was far more selective to propylene than ethylene, which implies that, if the two cycles equally contribute to the product distribution, most ethylene will be formed in the aromatic cycle[39]. The coexistence of the two cycles naturally renders them as competing[40]. In this spirit, one can speculate that a desired hydrocarbon range can be obtained by either stimulating or suppressing one over the over. Such co-catalytic features of HCP species during the MTH reaction were later theoretically verified by van Speybroeck and colleagues[41], indirectly reinforcing the concept of hybrid organic-inorganic nature of a working MTH catalyst, as originally proposed by Svelle and co-workers[36].

UV-visible DRS is possibly the most utilized spectroscopic technique for the characterization and identification of zeolite-trapped organics. The biggest advantage of UV-visible DRS is its ability to differentiate between carbocationic HCP species and their neutral counterparts. For instance, the absorption band of any arenium HCP cation is lower in energy than any electronic transition of its neutral counterpart. Moreover, UV-visible DRS provides insightful information regarding the zeolite framework dependent formation of deactivating species during the course of reaction. In general, multiple bands at around ≤295, 340–360, 385–410, 460–500 and ≥600 nm are observed during a MTH reaction and were typically attributed to neutral benzene/cyclopentadienyl species; dienylic carbocationic/methylbenzeniums (up to three methyl groups); highly methylated areniums (specifically hexamethylbenzenium ions, HMB^+); trienylic and methylated polyarenium ions, respectively (Fig. 3d,e)[25,26,42–47]. The formation and characteristics of these bands are quite unique depending on the zeolite framework topology and acidity; for instance, the specific role of alkyl cyclopentadienium ions over an MFI zeolite (for example, H-ZSM-5) was identified by Jentoft and Wulfers using in situ UV-visible DRS (Fig. 3d)[46]. Similarly, the Weckhuysen group identified the nature of governing active and deactivating methylated aromatic species during the MTH process over CHA zeolites (for example, H-SAPO-34 and H-SSZ-13) employing a combination of *operando* UV-visible DRS and online gas chromatography/mass spectrometry[13,42,47]. Using a similar strategy involving *operando* UV-visible DRS, the same group very recently monitored the formation of active HCP species and the accumulation of coke molecules during both H-ZSM-5 and Mg-ZSM-5-catalysed MTH[48]. Such spatiotemporal UV-visible spectroscopic approach reveals the formation of a coke front at the beginning of reactor bed, which travels towards the end until full deactivation. Magnesium modification resulted in slower progression of the coke front and higher olefin selectivity. However, identification/assignment of zeolite-trapped any organic reaction intermediates by UV-visible DRS in combination with theoretical calculations is not always straightforward and, to some extent, confusing. For example, HMB^+ and the 1-methylnaphthyl cation display a similar absorption band at ~390 nm (refs [41,44]). Unfortunately, both are probable intermediates of the MTH reaction, whereas HMB^+ is an active HCP species and the other is formed during the deactivation period[41]. This is the reason behind the enormous rise of utilization of solid-state NMR spectroscopy in recent years for the accurate structural elucidation of trapped organics within zeolites (vide supra)[13,14,17]. The combination of solid-state NMR with UV-visible DRS has made significant advancement by the groups of Hunger[18,25,43] and Haw[49–51].

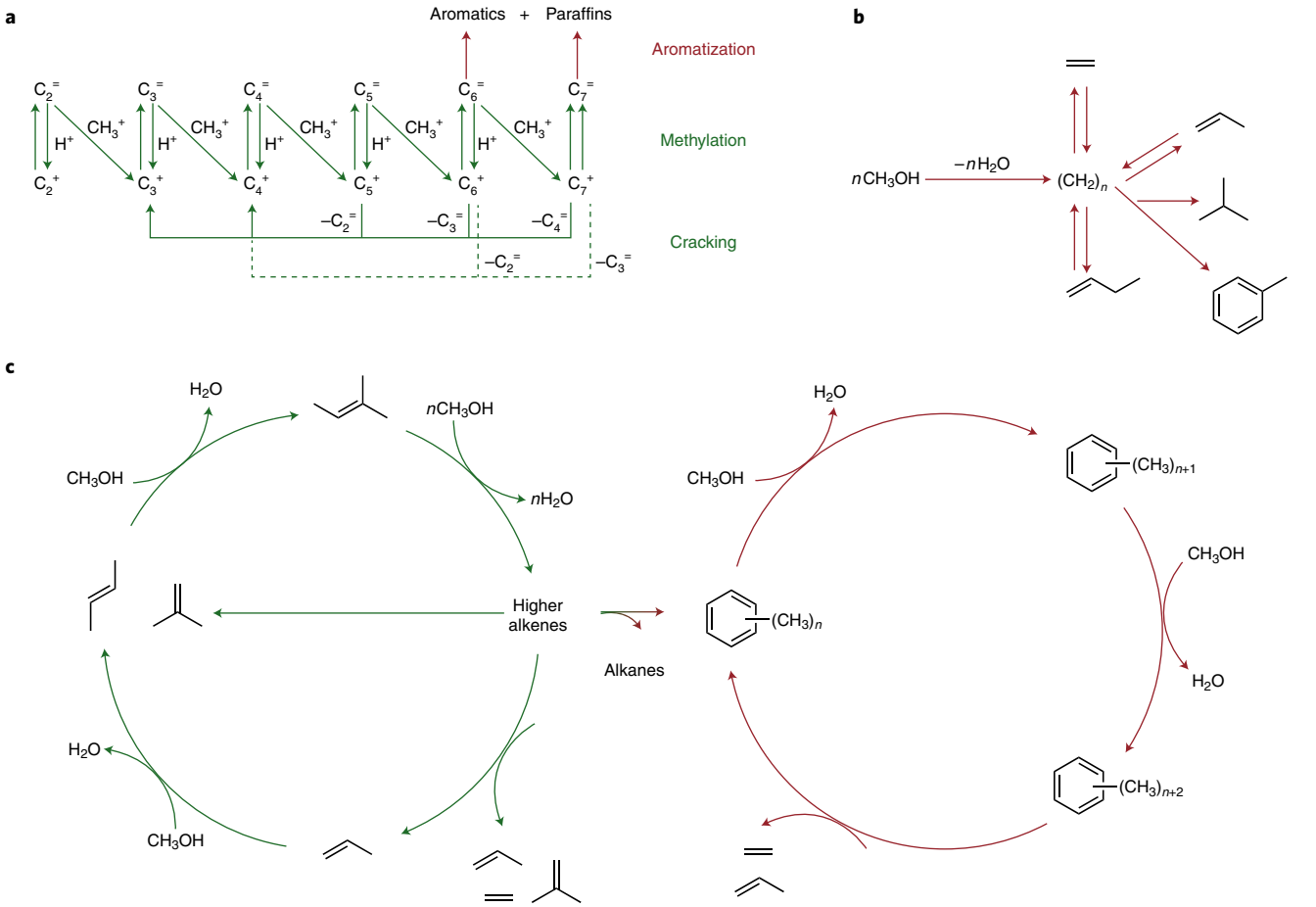

Fig. 4 | Steady-state mechanism development of the MTH process. a, Dessau and LaPierre described steady state kinetics of MTH reaction over ZSM-5 by a sequence of olefins methylation followed by their cracking or aromatization to give either olefins or aromatics. **b**, By contrast, Dahl and Kolboe investigating MTH over SAPO-34 introduced the HCP concept — an active intermediate of aromatic nature — through which light olefins are formed by dealkylation. **c**, The dual-cycle postulates that there are two competing cycles running in the zeolite channels governed by olefins and aromatics, both acting as co-catalysts for MTH and being active HCP species. Panel **a** adapted from ref. [35], Elsevier; panel **b** adapted from ref. [19], Springer; panel **c** adapted from ref. [5], Wiley.

Due to its capability to provide information at the molecular level, the utilization of solid-state NMR spectroscopy is increasing gradually in the field of heterogeneous catalysis[13]. Using ^{13}C-enriched methanol not only significantly increases NMR sensitivity, but also allows multi-dimensional solid-state NMR correlation experiments to be performed in order to construct the accurate molecular structures along with structural information of dominant carbenium ions involved in the HCP of the MTH-mechanism[6,18,49]. For instance, the alkylated cyclopentadienium ion was detected as the primary HCP species over HMB$^+$ within H-ZSM-5 and H-SSZ-13 zeolites during MTH reaction, whereas hexa-/hepta-methylbenzenium cations are widely acknowledged as the governing HCP species within SAPO-type molecular sieves (like SAPO-34, DNL-6) and H-Beta (Fig. 3f)[6,13,24,51–54]. This observation was quite consistent with the UV-visible DRS reports by the groups of Jentoft and Weckhuysen[13,42,47]. These results demonstrate that the formation of dominant carbenium HCP species is entirely dependent on the zeolite's framework and acidity.

In a nutshell, the scientific community now accepts that the direct mechanism exists during the early stages of MTO reaction and that HCP species vary depending on zeolite framework, acidity and reaction conditions. Numerous recent mechanistic reports provide solid experimental and spectroscopic evidence and the simultaneous existence of multiple direct C–C bond forming routes during the MTO reaction is quite likely[6].

Based on this mechanistic knowledge, several strategies can be put forward to drive selectivity of the process in different directions depending on the desired product. The first approach is related to the manipulation of the organic counterpart, that is, changing the concentration of olefin and/or aromatic species. Obviously, the second approach deals with the inorganic element and can be achieved by making use of catalyst engineering. Taking propylene and ethylene (and/or aromatics) yields as the measure of cycle dominance, we will now analyse how certain factors selectively propagate one cycle over the other.

Towards improved selectivity in MTH

When talking about catalyst and process design, the induction period was disregarded as a possible tool to manipulate both selectivity and lifetime because for a long time it was considered as a negligible part of the entire MTH mechanistic picture. Recent investigations indicated that formaldehyde — formed through disproportionation of methanol during direct C–C bond formation — causes catalyst deactivation via interaction with aromatic molecules resulting in the formation of polycondensed aromatics[55]. Besides, formaldehyde formation is accompanied with the production of CH_4 (ref. [56]). It thus becomes clear that in order to achieve better catalyst stability and selectivity, the induction period should be re-engineered to avoid formaldehyde formation. This issue can be addressed at both the catalyst and reactor level. At the reactor level,

utilization of a continuously stirred tank reactor (CSTR) instead of a plug flow reactor (PFR) leads to lower local methanol concentrations and lower oxygen containing species, thus mitigating catalyst deactivation[57]. Moreover, utilization of DME instead of methanol avoids the potential formation of formaldehyde and results in higher methylation rates in comparison to methanol, substantially prolonging catalyst lifetime[56]. At the catalyst level, it was proposed that addition of rare-earth oxides, such as Y_2O_3, should selectively decompose formaldehyde thus preventing its further interaction with aromatic species[58]. Utilization of DME (DME/water) instead of methanol seems to be the best solution, since apart from mitigating catalyst deactivation it decreases the overall heat release (the reaction enthalpy of DME dehydration is lower than that of methanol) making it more attractive from an industrial perspective[59].

Taking advantage of autocatalysis

Both olefins and aromatics are recognized as competitive co-catalysts, the excessive presence of a certain product promotes the cycle from which it originates[38,40]. So the most straightforward strategy to enhance the yield of olefins (propylene and butenes) or aromatics is to increase their concentration by co-processing them with methanol. Several works report the effect of co-feeding a wide range of olefins and/or aromatics with methanol on the product distribution, however, with the main aim to shed light on mechanism details[60,61].

In a wide range of temperatures and at different methanol conversion levels, co-feeding of toluene results in an increase of ethylene and methylbenzene concentration at the expense of propylene and higher olefins as a result of the aromatic cycle propagation[40,62–64]. This strategy can be used to respond to the constantly fluctuating market demands to produce a mixture of olefins with pre-assigned $C_2^=/C_3^=$ ratio. Olefins co-feeding turns out to be less straightforward and the propagation of the corresponding cycle depends on other parameters. The JGC corporation reported significantly enhanced propylene yield (up to 60–70%) when C_4–C_5 products were recycled with methanol feed at temperatures higher than 843 K (refs [65,66]). Co-feeding a small amount of propylene at low conversion levels at 548–623 K results in a higher contribution of the olefin cycle, confirmed by higher selectivity towards C_3^+ products[63], whereas at 723 K and higher conversion levels there is no notable effect of olefins co-feed[40]. In the first scenario, methylation reactions are promoted over cracking, therefore any inclusion of short chain olefins such as propylene results in a dramatic increase of C_3^+ products. At high methanol conversion levels (>70%), the olefinic cycle becomes more important[38], whereas further addition of olefins promotes both formation of higher olefins, which — with equal success — are either cracked or aromatized, thus contributing to both cycles. This brings another important conclusion: process parameters such as temperature and methanol space–time also contribute to the promotion of one cycle over the other when bed effects come into play. Temperature is another decisive parameter in determining the type of prevailing reactions. Higher temperatures promote cracking of higher olefins rather than their cyclization, which can be perceived as promotion of the olefinic cycle. Therefore, to maximize propylene production, the MTP process is carried out at temperatures higher than 723 K.

Influence of zeolite topology on product selectivity

The zeolite skeleton dictates its shape-selective properties, allowing the participation in the chemical reaction of only those molecules that are able to fit inside the zeolite pores[67]. This broad definition can be further subcategorized into reactant-, product- and transition-state selectivity; thus, being an inherent attribute of zeolitic materials, shape selectivity can be effectively utilized to propagate one cycle over another via product- and transition-state selectivity[68,69].

Small-pore 8-membered ring (8MR) zeolites are composed of large cavities interconnected by narrow window openings (Fig. 5a,b)[70,71]. Window openings are limited by eight atoms: big enough to let short-chain olefins pass through, but sufficiently small as to retain bigger molecules inside of their cages, thus creating an ideal playground to incubate the aromatic-based HCP[7]. In such an architecture, cavity dimensions can influence the nature of the aromatic intermediates (transition-state selectivity)[72], whereas window dimensions impose restrictions for the molecules formed inside (product selectivity). Thus, slight differences in both dimensions can affect product distribution and propylene/ethylene ratio, however, such dimensions guarantee high selectivity to short-chain olefins (up to 90%)[73]. Note that the HCP trapped inside also serves as a scaffold for the formation of polycondensed species, eventually leading to catalyst deactivation. The challenge for this type of zeolites is to achieve steady-state performance of the aromatic cycle by slowing down coke formation, accomplished by utilization of silicoaluminophosphates (SAPOs) with milder acidity[74]. On the other hand, steady-state performance with a constant coke content can be achieved by utilizing fluidized bed reactors, which additionally provide the advantage of a better heat dissipation[7]. Such reactor design, however, requires application of fluidizable catalysts; that is, with specific particle size and density. CHA — the most studied topology — is composed from cylinder-like cavities with big dimensions able to host aromatic molecules up to pyrene (Fig. 5a,b)[75]. Such large dimensions ensure long lifetime in comparison to other 8MR zeolites. Linked to the product distribution, the following conclusion can be drawn on the effect of cage dimensions: the more spacious is the cage the higher is selectivity to propylene[72,76,77]. Compared at the same temperature (350 and 400 °C), LEV with the smallest dimensions (7.5 × 6.5 Å) yields higher amount of ethylene, whereas more spacious CHA (10.9 × 6.7 Å) and AEI (12.7 × 11.6 Å) yield propylene[76]. The product distribution can be further linked to the confined aromatics; that is, steric limitations imposed by LEV favour formation of methylbenzenes with limited amount of methyl groups which are responsible for ethylene formation. The pear-shape of AEI is able to hold bulky aromatics, resulting in an unusually high selectivity to butenes (propylene/ethylene/butane = 2.8/1/1.1) at 400 °C (ref.[78]). Large cage dimensions do not guarantee high selectivity to propylene/butenes if combined with very narrow pores hindering diffusion of the latter[79]. An example is AFX (13.0 × 8.3 Å) with very small window-openings (3.4 × 3.6 Å) promoting rapid growth of polycondensed species and therefore fast deactivation[77]. Similarly, the more spacious cage of ERI delivers higher selectivity to ethylene in comparison to CHA, which might be due to narrower window openings of ERI (3.6 × 5.1 Å) in comparison to CHA (3.8 × 3.8 Å)[80].

Medium pore 10-membered ring (10MR) zeolites, on the other hand, are composed of straight and/or curved channels (Fig. 5c–f). In such structures, the aromatic cycle is only able to operate in the more spacious channel intersections[81,82]. Choosing zeolites with absence of those ensures discarding the aromatic cycle. One-dimensional ZSM-22 with TON topology was the first zeolite for which suppression of the aromatic cycle was postulated[83], the same observations latter being made for other one-dimensional 10MR zeolites (Fig. 5c,d)[84,85]. The prevalence of the olefinic cycle combined with product shape selectivity results in the predominant formation of C_{5+} products ranging from 50 up to 75% depending on the conversion levels. The obtained product mixture rather meets the requirements for gasoline (after hydrogenation step), with the formation of propylene being fairly low. Selectivity to propylene can be further improved by optimizing acidic properties of zeolites leading to up to 53% of propylene selectivity at 450 °C (ref. [86]), while optimization of textural properties dramatically prolongs catalyst lifetime[87]. For zeolites with intersections, two cycles work in parallel, and propagation of one cycle over the other can be achieved by other means (Fig. 5e,f)[88].

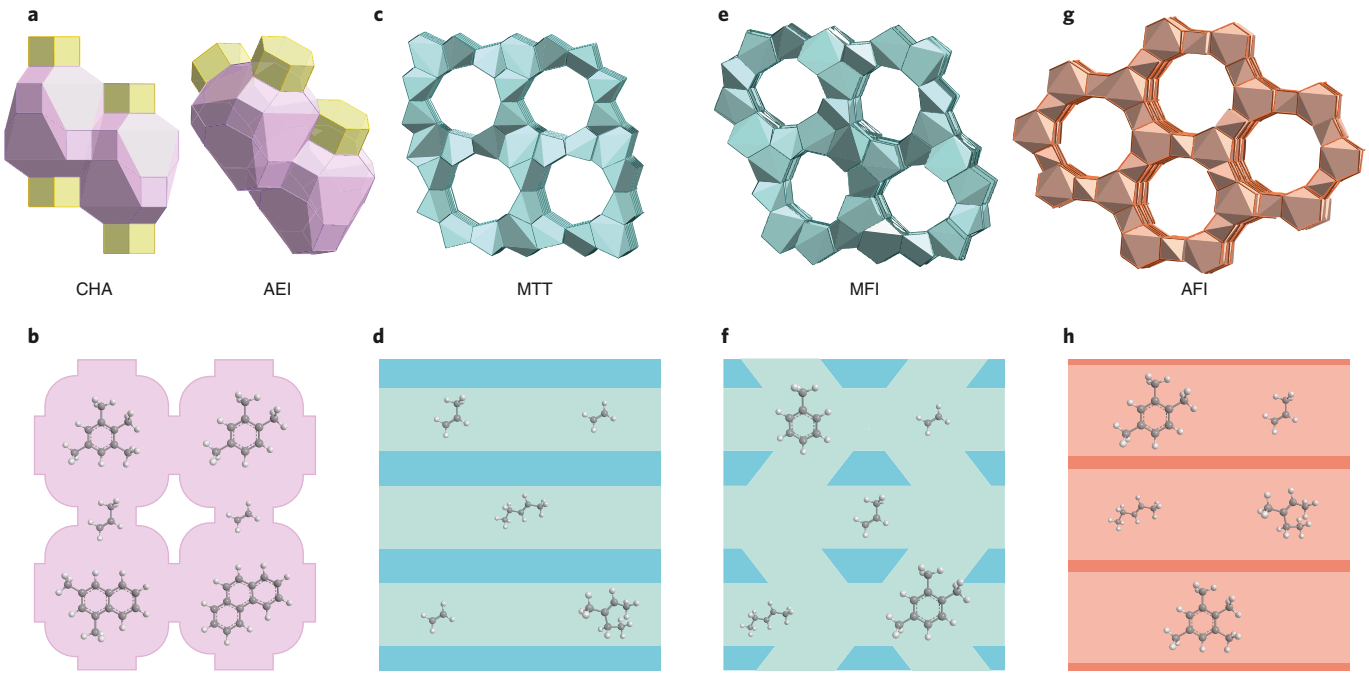

Fig. 5 | Impact of topology on cycles propagation. a,**b**, 8-membered ring zeolites are composed of large cavities with small window openings; in such structures aromatics can be formed but cannot escape the cage. The aromatic cycle is prevailing and such topologies are characterized by high selectivity to short-chain olefins. **c**,**d**, 1D 10-membered ring zeolites cannot accommodate aromatic molecules, therefore the aromatic cycle is suppressed in such type of topology. The product distribution is characterized by a gasoline range of hydrocarbons. **e**, The 3D 10-membered ring MFI structure is described by two types of channels — straight and sinusoidal — forming relatively spacious intersections, which can host the aromatic cycle. **f**, Both the aromatic and olefinic cycles are running in zeolite channels and the product is characterized by the presence of a wide range of hydrocarbons. **g**,**h**, The channels of 12-membered ring zeolites are rather big and can host aromatic hydrocarbons, therefore the aromatic cycle can run inside the channels of a 1D AFI zeolite.

Logically, further increase of the number of T-atoms in window openings corresponding to 12-membered ring (12MR) zeolites allows the aromatic cycle to proceed inside the zeolite channels. Therefore, 1D SSZ-24 with tubular channels comparable to the size of CHA cavities is almost exclusively selective to aromatics at low conversion levels (~90%) and >26% at high conversion levels (Fig. 5g,h)[89]. Besides, wider window dimensions result in the formation of much more alkylated aromatics for zeolite beta and MOR (mainly penta- and hexamethylbenzene) in comparison to 10MR ZSM-5 (mainly BTX[90]). Thus, in 8MR and 12MR zeolites composed of large cavities and channels respectively, the aromatic cycle is preferred. Nevertheless, being imprisoned by narrow 8MR windows it selectively produces short chain olefins in one case, and heavy aromatics with no such restrictions.

Impact of acidity on stability and product selectivity

Concentration, location and strength of acid sites are the three most important parameters in defining the overall acidity in zeolites. Concentration of Brønsted acid sites is primarily linked to the amount of Al in the zeolite. A literature survey reveals a linear correlation between propylene selectivity and Si/Al ratio, while a notable reduction in aromatics selectivity corresponds to the decrease of aluminium content in the zeolite (established for MFI but also holding for other topologies)[91–96]. Opposite trends strongly evidence the competing nature of the two cycles and that higher acid site density propagates the aromatic cycle (Fig. 6a–d). An increase of aluminium content enhances the chance of reactant molecules to interact with each other, thus increasing the chance to form aromatics and ethylene — the product of the aromatic cycle[97]. The observed trends also account for the improved selectivity to propylene for post-synthetically modified catalysts with different elements as well demetalated zeolites. It has been extensively shown that phosphatation and incorporation of alkaline-earth metals lead to a significant reduction of Brønsted acidity and its effect can be regarded as an increase in the Si/Al ratio[98,99]. Yarulina et al.[98] have shown that calcium incorporation results in an almost 10-fold reduction of Brønsted acidity. As a consequence, hydride transfer and cyclization reactions were suppressed, resulting in very low amounts of paraffins and aromatics and maximizing propylene yield up to 53%. Apart from the development of the second type of porosity improving diffusional properties of zeolites, desilication and dealumination of zeolites can be also viewed as an instrument to dilute acid site density and inhibit secondary reactions[94]. Zeolites with similar bulk properties can still exhibit substantially different catalytic behaviour, which is a side effect of a heterogeneous distribution of aluminium within the crystal, also called aluminium zoning. For example, an aluminium-rich rim is characteristic for ZSM-5 crystals synthesized using TPA^+ as structure-directing agent[100]. Aluminium-zoning obviously can be considered as a local enhancement of acid density, which, as explained above, promotes the aromatic cycle. Hydrothermal synthesis conditions and the precursor composition mixture can also promote different locations of aluminium within the crystal lattice. Here it should be pointed out that the definition of aluminium zoning used in the following describes a gradient in the number of aluminium atoms per unit volume, not a distribution gradient of aluminium over the available T sites per unit cell. Aluminium zoning in zeolites has been observed since the 1970s[101]. Around that time and in the following years different distributions and effects were observed and in 1993 Althoff and co-workers published[102] a systematic study of the parameters influencing aluminium zoning.

Besides influencing desilication and dealumination, because strength and number of catalytically active sites in zeolites affect the effective diffusion path of reactants, the presence and distribution of aluminium in the zeolite framework also directly

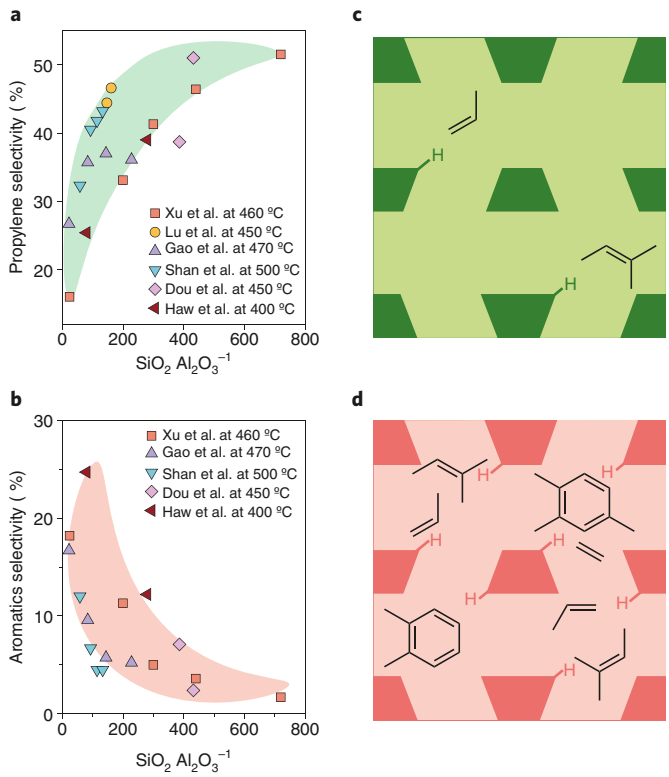

Fig. 6 | Impact of acidity on cycles propagation. a,**b**, A literature survey[91–96] reveals a noticeable increase of propylene (**a**) and a reduction of aromatics (**b**) formed along with an increase of the SiO_2/Al_2O_3 ratio for microporous ZSM-5 zeolites tested in the MTH reaction at 673–773 K and in the wide range of WHSV. Opposite trends highlight the competing nature of aromatics and olefins. **c**, A significant reduction of aluminium in the zeolite framework leads to a decrease of Brønsted acid site (BAS) density, consequently propagating the olefinic cycle as a result of a decreased amount of secondary reactions leading to olefins cyclization and aromatic formation. **d**, An increase of acid site density results in a higher probability for olefins to interact forming aromatic molecules. A reduction of Brønsted acidity can be achieved by post-synthetic modification with alkaline earth metals or demetallation procedures (**c**,**d**) leading to similar trends.

affects catalytic performance (Fig. 6). It was shown that several acid-catalysed reactions preferentially occur at the edges of large ZSM-5 crystals: in 2007, Roeffaers and colleagues[103] applied in situ fluorescence microscopy to monitor catalytic, condensed-phase reactions in individual zeolite crystals. Specifically, they utilized the (acid-catalysed) formation of chromophores during self-condensation of furfuryl alcohol to visualize the time-dependent distribution of the fluorescent reaction products. With their study, they showed that the presence of sub-units in large, coffin-shaped ZSM-5 crystals is relevant to catalysis, and proposed that the interfaces between the components act as diffusion barriers. The authors also observed unusual behavior of certain crystals, showing intense fluorescence emission confined to the outer surface of specific facets of the ZSM-5 crystals and linked this unusually intense emission to aluminium zoning. In the same year Kox and co-workers used in-situ UV-Vis microspectroscopy to study the oligomerization of styrene occurring in the micropores of ZSM-5 zeolite crystals[104], linking reaction kinetics to the diffusion and catalytic properties of straight and zigzag channels in large ZSM-5 zeolite crystals. One year later Tzoulaki et al.[105] studied the diffusion properties of large (aluminium-free) silicalite-1 crystals using interference microscopy for monitoring time-dependent concentration profiles during molecular uptake and release and found no evidence for a significant effect of internal transport resistances (at the interface of sub-units) or surface barriers on mass transport in these crystals. They therefore concluded that an inhomogeneous aluminium distribution — preferentially located close to the surface and at the interfaces of the crystal segments — enhances catalytic activity and coke formation, and is responsible for the observed diffusion barriers. In line with this hypothesis, later in 2008 Mores et al.[106] confirmed the heterogeneous distribution of coke as a function of reaction time and temperature in large H-ZSM-5 and H-SAPO-34 crystals during the MTO reaction by a combination of in situ UV-visible and confocal fluorescence microscopy. Three years later Weckhuysen and colleagues[107] showed that with decreasing aluminium concentration in large MFI crystals, coke formation decreases as well. Furthermore, a higher Brønsted acid site density did not influence the type of coke species generated, but instead increased the rate of formation of methyl-substituted aromatic species and the subsequent growth towards larger coke species. One year later, in 2012, Chen and co-workers[74] reviewed the effect of acid site density, acid site strength and the role of coke formation on deactivation of SAPO zeolites and in 2015 Olsbye et al.[6] reviewed the MTH process *inter alia* discussing catalyst deactivation by coke formation.

Catalyst deactivation by (hydro-) carbon residues is an important deactivation pathway in MTH. However, as discussed, after the formation of the first C–C bond species hydrocarbons are formed according to the autocatalytic dual-cycle concept, which implies that hydrocarbon species can be both activating and deactivating species[6]. It is therefore interesting to obtain insights about the nature and location of the first seeds of coke in zeolites. Intuitively one would expect the first coke species to form in regions with (i) highest accessibility and (ii) highest activity — both of which can be influenced by aluminium gradients in the catalyst. However, resolving the location of the first coke species formed at the length scale of nanometers and relating it to (local) aluminium gradients remains extremely challenging. Recently, the first use of atom probe tomography (APT) to investigate the 3D distribution of elements in zeolites at the sub-nm scale has been reported (Fig. 7)[108,109]. In 2016 Schmidt et al.[109] used APT to study coke formation and its relation to inhomogeneous aluminium distribution in large ZSM-5 crystals after MTH (using ^{13}C-labelled methanol to distinguish the formed coke species from contaminations). APT samples were taken from the (aluminium rich) surface and the (aluminium poor) core of the ZSM-5 crystal showing a clear correlation of coke formation and Brønsted acid site density. The authors reported the presence of carbon clusters (using the term cluster as synonym for a group of closely positioned atoms), which revealed insights into the coke formation mechanism, showing that the coke clusters form preferentially around areas with elevated aluminium content, even in the aluminium-poor core of the crystal. The median size of the observed ^{13}C clusters was around 36–69 carbon atoms, which suggests that these clusters could contain several occluded aromatic species. Independent of the location of the APT (that is, taken from the surface or core of the large ZSM crystal), ^{13}C clusters were found in each sample, suggesting that in the beginning of the reaction methanol is present throughout the crystal (Fig. 7). As the MTH reaction and catalyst deactivation progress these large clusters merge into the coke rich regions observed for example, in the surface of large ZSM crystals, that is, in regions of elevated aluminium concentrations. These observations were found to be in line with the previously suggested mechanism of coke formation in ZSM-5 during MTH (see refs[6,93–96], among others).

Variation in silicon sources was taken as a strategy by Wang et al.[81] to obtain ZSM-5 zeolites with acid sites located either in intersections or in straight and sinusoidal channels. Having the same Si/Al ratio, zeolites with acid sites located in channels exhibited

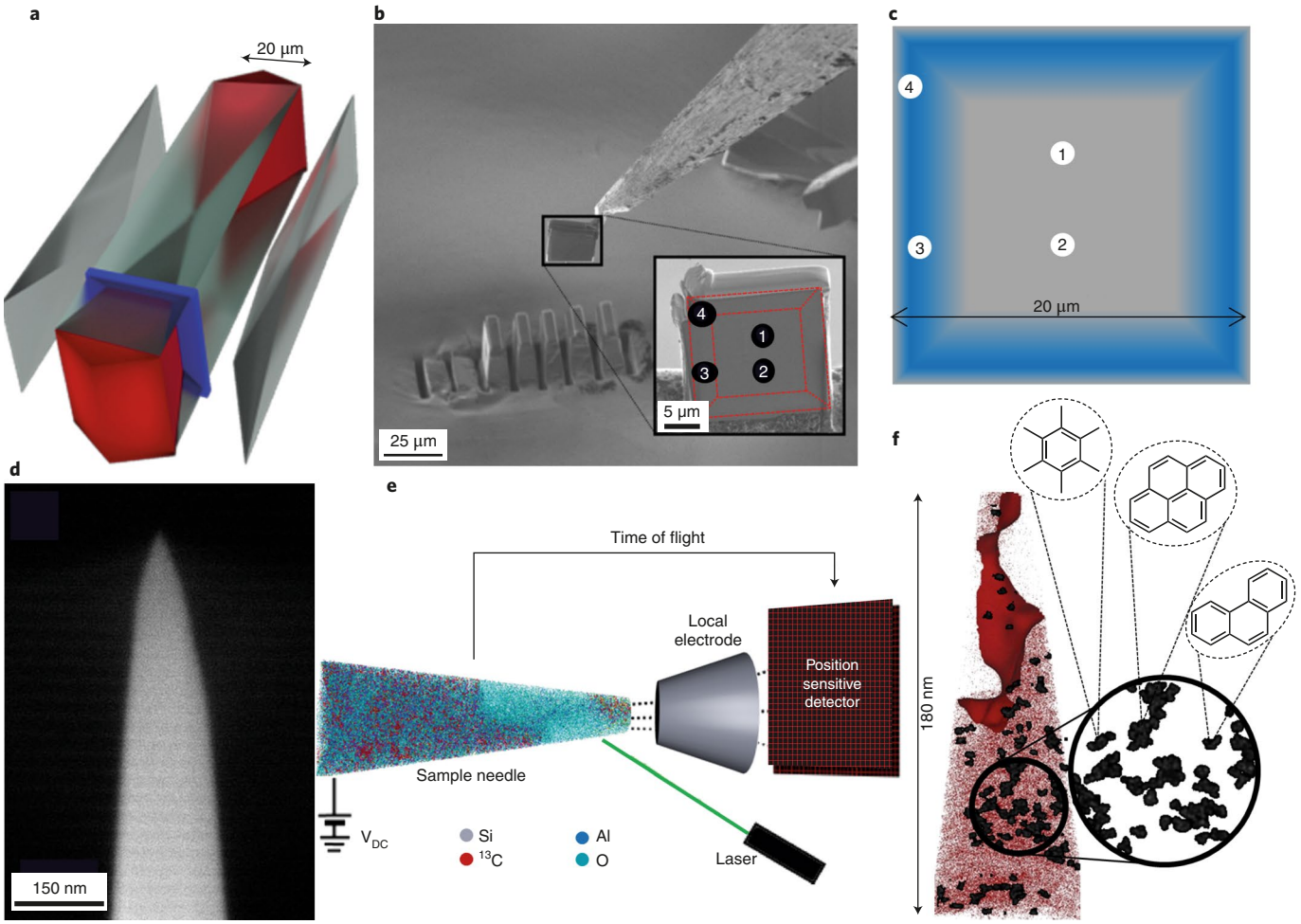

Fig. 7 | Resolving the location of the first coke species formed during the MTH process using APT. a–f, APT was used to study coke formation and its relation to the inhomogeneous Al distribution in large ZSM-5 crystals after MTH reaction[109]. A cross section was prepared from a large ZSM-5 crystal after MTH reaction using ^{13}C-labelled methanol by focused ion beam (FIB) cutting (**a** and **b**). For APT four samples (needles) were taken using FIB cutting from different regions of the crystal cross-section considering aluminium zoning: high aluminium concentrations are indicated in blue in panel **c** also showing the position of the samples investigated by APT. A typical needle is shown in panel **d**. APT then allowed mapping of the 3D distribution of Si, Al, O, and ^{13}C atoms within each needle (**e**). Statistical analysis of the distribution of the ^{13}C atoms revealed the presence of carbon clusters indicating the regions of first coke formation in the catalyst (**f**). Figure adapted from ref. [109], Wiley.

significantly higher selectivity to propylene and longer lifetime. Such a location of aluminium inhibited the aromatic cycle which is operative in the more spacious intersections and resulted in the similar effect as if utilization of 1D 10MR zeolites.

Finally, the effect of acid strength was extensively compared over aluminosilicates and their SAPO versions. The general observation is that $C_3^=/C_2^=$ ratio and methanol conversion capacity over SAPOs is higher, suggesting lower formation rates of polycondensed species[110]; however, any speculation on the dominating cycle is rather dubious as it was studied over 8MR zeolites where the aromatic cycle is prevailing due to topology features. A similar comparison performed for 12MR zeolites reveals that although the product distribution is dominated by aromatics for H-SSZ-24 (AFI), H-SAPO-5 (AFI) displays high selectivity to butenes and shows almost no aromatics. A combination of co-reaction experiments and theoretical calculations reveals that the acid strength has a profound effect on the reactivity of co-catalytic HCP species[89]. For H-SSZ-24, benzene methylation is significantly higher than that for propylene bringing the aromatic cycle into the dominating role — in sharp contrast to H-SAPO-5 exhibiting similar rates for olefins and aromatics methylation[111].

Host–guest interactions

Throughout this Review, zeolites' framework topology and acidity dependent formation of products (both olefins and HCP species) during the MTH reaction have been highlighted. This feature could easily be linked to the host–guest chemistry between inorganic zeolite and organic HCP species during the reaction. More importantly, it also provides the necessary evidence in support of the hybrid organic–inorganic nature of working MTH catalyst (*vide supra*)[36,41]. During evaluation by Goetze and colleagues[112] of HCP species throughout the MTH process over three small-pore and eight-ring windows zeolites (CHA, DDR, LEV), generation of non-identical organics was noticed due to very small differences in cage size, shape and pore structure of the zeolite frameworks. By encompassing a combination of multivariate analysis of *operando* UV-visible spectroscopy and online gas chromatography, along with bulk chemical analysis of the hydrocarbon deposits by GC/MS of extracted coke species and thermogravimetric analysis, it was observed that CHA, DDR and LEV preferentially formed alkylated aromatics and pyrene, 1-methylnaphthalene, and methylated benzene and naphthalene, respectively. The molecular dimension of these retained organic species (that is, the guest molecule) is

comparable to the dimensions of the respective zeolite cages (that is, the host molecule). As a result, the lattices of all three zeolites were expanded during the MTH process, as revealed by *operando* X-ray diffraction (XRD)[113]. The expansion of the *c*-axis of the CHA and LEV lattices (that is, longitudinal direction of their cages) is about 0.9% and 0.5% during the MTH process, which is more than in the direction of *a*- and *b*-axes (that is, in the direction of the width of the cage). On the contrary, relatively further expansion in the direction of *a*- and *b*-axes of DDR lattice (that is, 0.5% compared to 0.3% along the *c*-axis) means it becomes wider during the MTH process due to coke deposition, whereas both CHA and LEV lattices become longer. This observation provides further evidence for distinctive host–guest chemistry between zeolite and retained organics during catalysis. To further elucidate the concept of host–guest interactions during catalysis, the report from Liu et al. should be mentioned[72]. With the help of isotopic tracing and theoretical calculations, they showed that the cavity size of different SAPO molecular bearing identical 8MR pore openings (that is, SAPO-35, SAPO-34, and DNL-6) control the molecular size as well as reactivity of the confined HCP species, which eventually influences the conversion and selectivity of olefins during the MTH reaction[72]. Although such confined/retained/trapped organics within the zeolite framework are believed to be rigid in nature, this is not completely true. Although elucidating the reaction mechanisms of zeolite-catalysed MTH (Fig. 3a,c) and alkylation of aromatics, the same group adapted different solid-state NMR magnetization transfer techniques that were previously developed for spectral separation of biomolecules on the basis of their mobility in order to distinguish between mobile (that is, a molecule or group with fast tumbling or rotation) and rigid (that is, molecule physisorbed in/on zeolite) species (both were trapped within zeolite)[13,114]. However, this host–guest feature of zeolite catalysis has recently been developed and demands further research activities to confirm its implications in the actual process. Nevertheless, it contributes to the fundamental understandings of the zeolite-catalysed hydrocarbon conversion chemistry.

Summary and outlook

After more than 40 years, the methanol-to-hydrocarbons process remains as one of the most popular topics of research within the zeolite catalysis community. The recent industrial implementation, with several new commercial plants already running, has triggered even more attention from the academic and industrial communities. In this line, the interest towards the formation of the direct C–C bond, which until very recently was believed to be due to impurities, has risen over the last few years. The combined effort by several research groups helped identify several feasible low-barrier direct coupling pathways for this key mechanistic step, although feedstock impurities (in principle) could still shorten the induction period[115]. Among them, formaldehyde formed through disproportionation of methanol was identified as a deactivating species due to its high reactivity with aromatics and the undesired formation of polyaromatic species. This important discovery calls for new reactor concepts where reactant feeding should be performed carefully to avoid high concentrations of methanol and the consequences thereof, including heat effects.

The next mechanistic step, the dual-cycle, is now better understood and can be viewed as the main machine for controlling lifetime and selectivity to the desired products. The combination of NMR and UV-visible DRS helped pinpoint not only active intermediates, but also deactivating ones, although there is a fine line between them. It has been extensively shown that deactivating species can become reaction intermediates if, for example, higher reaction temperatures are used. Moreover, their reactivity depends on zeolite topology: channel/cage dimensions can cause spatial restrictions preventing certain intermediates to participate in the mechanistic cycle. In 2012, Olsbye et al.[5] posed the question whether the two cycles — olefinic and aromatic — can be promoted one over another and whether one of them can independently exist. The challenge has been partially addressed: recent catalytic results demonstrate that it is possible to extend catalyst lifetime up to approximately 1 kg CH_3OH per gram zeolite while maintaining high propylene selectivities (>50%). However, it should be further clarified if deactivating species in these cases are also of aromatic nature.

Considering that for both cycles the active intermediates act as co-catalysts, reaction conditions (temperature and methanol partial pressure), feed composition (that is, the presence of olefinic or aromatic co-feed), zeolite topology and acidity can be tuned to further enhance performance. Having this said, most of the efforts over the last few years have been directed towards the selective formation of propylene (the main product from the olefinic cycle). In a potential scenario of lack of ethylene, it would be desirable to apply similar concepts towards the selective formation of this highly important chemical. How to achieve this objective without compromising catalyst lifetime is however still an open question, as ethylene is the main product of the aromatic cycle, its formation would in principle always be accompanied by a high rate of formation of aromatics. Along the same line, considering potential fluctuations in the olefin market, in an ideal scenario there should be a catalyst whose selectivity can easily be tuned by changing the reaction conditions. Here the best solutions seem to go in the direction of co-feeding the required products to promote the cycle of interest. This aspect again calls for additional efforts at the reactor level.

In summary, in our opinion, MTH is still a fascinating research topic with a number of scientific and engineering challenges to be addressed in the near future. Surprisingly, the latter (engineering) challenges have hardly been touched upon in the open literature, while these have been key in the success of the currently most applied MTH technology, which relies on the fast deactivating SAPO-34 and on fluidized bed technology. On a more fundamental note, we are looking forward to seeing the implications that the recent discoveries in MTH chemistry may have on other high temperature hydrocarbon chemistries, such as catalytic cracking and even direct methane activation, as well as bifunctional catalysis concepts, in which MTH chemistry may play an instrumental role. Indeed, the combination of zeolites with other functionalities opens new avenues for the direct conversion of CO_2 or syngas to olefins, hydrocarbons and aromatics[116,117]. In such a bifunctional systems, CO_2 or CO are first hydrogenated to methanol which is subsequently converted to hydrocarbons, the zeolite of choice being responsible for the second step. This is a rather promising concept, yet there are a number of obstacles to overcome, such as overhydrogenation of olefins to paraffins, high selectivity to CO and methane associated with metal functionality and how to find a proper catalyst matching in terms of deactivation.

Received: 6 February 2018; Accepted: 18 April 2018;
Published online: 12 June 2018

References

1. Chang, C. D. & Lang, W. H. Process for manufacturing olefins. US patent US4025576 A (1977).
2. Vogt, E. T. C. & Weckhuysen, B. M. Fluid catalytic cracking: recent developments on the grand old lady of zeolite catalysis. *Chem. Soc. Rev.* **44**, 7342–7370 (2015).
3. Mitchell, S. et al. Structural analysis of hierarchically organized zeolites. *Nat. Comm* **6**, 8633–8647 (2015).
4. Stöcker, M. Methanol-to-hydrocarbons: catalytic materials and their behavior. *Microporous Mesoporous Mater.* **29**, 3–48 (1999).
A review covering the main achievements in catalyst design and mechanism understanding of methanol-to-hydrocarbons process over the last century.
5. Olsbye, U. et al. Conversion of methanol to hydrocarbons: how zeolite cavity and pore size controls product selectivity. *Angew. Chem. Int. Ed.* **51**, 5810–5831 (2012).

A methanol-to-hydrocarbons review dedicated to mechanism understanding and describing main parameters affecting selectivty to hydrocarbons.
6. Olsbye, U. et al. The formation and degradation of active species during methanol conversion over protonated zeotype catalysts. *Chem. Soc. Rev.* **44**, 7155–7176 (2015).
7. Tian, P., Wei, Y., Ye, M. & Liu, Z. Methanol to olefins (MTO): from fundamentals to commercialization. *ACS Catal* **5**, 1922–1938 (2015).
8. Ilias, S. & Bhan, A. Mechanism of the catalytic conversion of methanol to hydrocarbons. *ACS Catal* **3**, 18–31 (2013).
9. Van Speybroeck, V. et al. First principle chemical kinetics in zeolites: the methanol-to-olefin process as a case study. *Chem. Soc. Rev.* **43**, 7326–7357 (2014).
10. Schulz, H. About the mechanism of methanol conversion on zeolites. *Catal. Lett.* (2018).
11. Yamazaki, H. et al. Evidence for a "carbene-like" intermediate during the reaction of methoxy species with light alkenes on H-ZSM-5. *Angew. Chem. Int. Ed.* **50**, 1853–1856 (2011).
12. Yamazaki, H. et al. Direct production of propene from methoxy species and dimethyl ether over H-ZSM-5. *J. Phys. Chem. C* **116**, 24091–24097 (2012).
13. Chowdhury, A. D. et al. Initial carbon–carbon bond formation during the early stages of the methanol-to-olefin process proven by zeolite-trapped acetate and methyl acetate. *Angew. Chem. Int. Ed.* **55**, 15840–15845 (2016). **An in-depth mechanistic investigation providing spectroscopic evidence in support of the Koch-carbonylation mechanism of the methanol-to-hydrocarbon reaction**.
14. Wu, X. et al. Direct mechanism of the first carbon–carbon bond formation in the methanol-to-hydrocarbons process. *Angew. Chem. Int. Ed.* **56**, 9039–9043 (2017).
15. Lercher, J. A. New Lewis acid catalyzed pathway to carbon–carbon bonds from methanol. *ACS Cent. Sci.* **1**, 350–351 (2015).
16. Liu, Y. et al. Formation mechanism of the first carbon–carbon bond and the first olefin in the methanol conversion into hydrocarbons. *Angew. Chem. Int. Ed.* **55**, 5723–5726 (2016).
17. Comas-Vives, A., Valla, M., Copéret, C. & Sautet, P. Cooperativity between Al sites promotes hydrogen transfer and carbon — carbon bond formation upon dimethyl ether activation on alumina. *ACS Cent. Sci.* **1**, 313–319 (2015).
18. Wang, W. & Hunger, M. Reactivity of surface alkoxy species on acidic zeolite catalysts. *Acc. Chem. Res.* **41**, 895–904 (2008). **An in-depth review providing versatile reactivity aspects of surface-methoxy species during zeolite catalyzed hydrocarbon conversion**.
19. Dahl, I. M. & Kolboe, S. On the reaction mechanism for propene formation in the MTO reaction over SAPO-34. *Catalysis Lett.* **20**, 329–336 (1993). **This article illustrates the concept of hydrocarbon pool species during zeolite catalyzed methanol-to-hydrocarbon process**.
20. Song, W., Marcus, D. M., Fu, H., Ehresmann, J. O. & Haw, J. F. An oft-studied reaction that may never have been: direct catalytic conversion of methanol or dimethyl ether to hydrocarbons on the solid acids HZSM-5 or HSAPO-34. *J. Am. Chem. Soc.* **124**, 3844–3845 (2002).
21. Lesthaeghe, D., Van Speybroeck, V., Marin, G. B. & Waroquier, M. What role do oxonium ions and oxonium ylides play in the ZSM-5 catalysed methanol-to-olefin process? *Chem. Phys. Lett.* **417**, 309–315 (2006).
22. Lesthaeghe, D., Van Speybroeck, V., Marin, G. B. & Waroquier, M. The rise and fall of direct mechanisms in methanol-to-olefin catalysis: an overview of theoretical contributions. *Ind. Eng. Chem. Res.* **46**, 8832–8838 (2007).
23. Jiang, Y. et al. Effect of organic impurities on the hydrocarbon formation via the decomposition of surface methoxy groups on acidic zeolite catalysts. *J. Catal.* **238**, 21–27 (2006).
24. Dai, W. et al. Understanding the early stages of the methanol-to-olefin Conversion on H — SAPO-34. *ACS Catal* **5**, 317–326 (2014).
25. Dai, W., Wu, G., Li, L., Guan, N. & Hunger, M. Mechanisms of the deactivation of SAPO-34 materials with different crystal sizes applied as MTO catalysts. *ACS Catal* **3**, 588–596 (2013).
26. Jiang, Y., Hunger, M. & Wang, W. On the reactivity of surface methoxy species in acidic zeolites. *J. Am. Chem. Soc.* **128**, 11679–11692 (2006).
27. Wang, W., Buchholz, A., Seiler, M. & Hunger, M. Evidence for an initiation of the methanol-to-olefin process by reactive surface methoxy groups on acidic zeolite catalysts. *J. Am. Chem. Soc.* **125**, 15260–15267 (2003).
28. Li, J. et al. A route to form initial hydrocarbon pool species in methanol conversion to olefins over zeolites. *J. Catal.* **317**, 277–283 (2014).
29. Wei, Z. et al. Methane formation mechanism in the initial methanol-to-olefins process catalyzed by SAPO-34. *Catal. Sci. Tech* **6**, 5526–5533 (2016).
30. Plessow, P. N. & Studt, F. Unraveling the mechanism of the initiation reaction of the methanol to olefins process using *ab Initio* and DFT calculations. *ACS Catal* **7**, 7987–7994 (2017).
31. Kazansky, V. & Senchenya, I. N. Quantum chemical study of the electronic structure and geometry of surface alkoxy groups as probable active intermediates of heterogeneous acidic catalysts: what are the adsorbed carbenium ions? *J. Catal.* **119**, 108–120 (1989).
32. Salehirad, F. & Anderson, M. W. Solid-state ^{13}C MAS NMR study of methanol-to-hydrocarbon chemistry over H-SAPO-34. *J. Catal.* **314**, 301–314 (1996).
33. Hutchings, G. J., Gottschalk, F., Hall, M. V. Ml & Hunter, R. Hydrocarbon formation from methylating agents over the zeolite catalyst ZSM-5. Comments on the mechanism of carbon–carbon bond and methane formation. *J. Chem. Soc. Faraday Trans.* **83**, 571–583 (1987).
34. Plessow, P. N. & Studt, F. Theoretical insights into the effect of the framework on the initiation mechanism of the MTO process. *Catal. Lett.* **148**, 1246–1253 (2018).
35. Dessau, R. M. & Lapierre, R. B. On the mechanism of methanol conversion to hydrocarbons over HZSM-5. *J. Catal.* **78**, 136–141 (1982).
36. Svelle, S. et al. Conversion of methanol into hydrocarbons over zeolite H-ZSM-5: ethene formation is mechanistically separated from the formation of higher alkenes. *J. Am. Chem. Soc.* **128**, 14770–14771 (2006).
37. Bjørgen, M. et al. Conversion of methanol to hydrocarbons over zeolite H-ZSM-5: on the origin of the olefinic species. *J. Catal.* **249**, 195–207 (2007).
38. Sun, X. et al. On reaction pathways in the conversion of methanol to hydrocarbons on HZSM-5. *J. Catal.* **317**, 185–197 (2014).
39. Wang, S. et al. Polymethylbenzene or alkene cycle? theoretical study on their contribution to the process of methanol to olefins over H-ZSM-5 zeolite. *J. Phys. Chem. C* **119**, 28482–28498 (2015).
40. Sun, X. et al. On the impact of co-feeding aromatics and olefins for the methanol-to-olefins reaction on HZSM-5. *J. Catal.* **314**, 21–31 (2014). **Seminal kinetic investigations demonstrating the autocatalytic nature of the mechanism and discussing the effect of the feed composition on the dominant reaction pathways**.
41. Van Speybroeck, V. et al. Mechanistic studies on chabazite-type methanol-to-olefin catalysts: insights from time-resolved UV/Vis microspectroscopy combined with theoretical simulations. *ChemCatChem* **5**, 173–184 (2013).
42. Borodina, E. et al. Influence of the reaction temperature on the nature of the active and deactivating species during methanol to olefins conversion over H-SSZ-13. *ACS Catal* **5**, 992–1003 (2015).
43. Dai, W. et al. Intermediates and dominating reaction mechanism during the early period of the methanol-to-olefin conversion on SAPO-41. *J. Phys. Chem. C* **119**, 2637–2645 (2015).
44. Hemelsoet, K. et al. Identification of intermediates in zeolite-catalyzed reactions by *in situ* UV/Vis microspectroscopy and a complementary set of molecular simulations. *Chem. Eur. J* **19**, 16595–16606 (2013).
45. Qian, Q. et al. Single-particle spectroscopy of alcohol-to-olefins over SAPO-34 at different reaction stages: crystal accessibility and hydrocarbons reactivity. *ChemCatChem* **6**, 772–783 (2014).
46. Wulfers, M. J. & Jentoft, F. C. The role of cyclopentadienium ions in methanol-to-hydrocarbons chemistry. *ACS Catal* **4**, 3521–3532 (2014).
47. Borodina, E. et al. Influence of the reaction temperature on the nature of the active and deactivating species during methanol-to-olefins conversion over H-SAPO-34. *ACS Catal* **7**, 5268–5281 (2017).
48. Goetze, J. & Weckhuysen, B. M. Spatiotemporal coke formation over zeolite ZSM-5 during the methanol-to-olefins process as studied with operando UV-vis spectroscopy: a comparison between H-ZSM-5 and Mg-ZSM-5. *Catal. Sci. Technol* **8**, 1632–1644 (2018).
49. Haw, J. F., Song, W., Marcus, D. M. & Nicholas, J. B. The mechanism of methanol to hydrocarbon catalysis. *Acc. Chem. Res.* **36**, 317–326 (2003).
50. Xu, T. et al. Synthesis of a benzenium ion in a zeolite with use of a catalytic flow reactor. *J. Am. Chem. Soc.* **120**, 4025–4026 (1998).
51. Haw, J. F. et al. Roles for cyclopentenyl cations in the synthesis of hydrocarbons from methanol on zeolite catalyst HZSM-5. *J. Am. Chem. Soc.* **122**, 4763–4775 (2000).
52. Li, J. et al. Observation of heptamethylbenzenium cation over SAPO-type molecular sieve DNL-6 under real MTO conversion conditions. *J. Am. Chem. Soc.* **134**, 836–839 (2012).
53. Xu, S. et al. Direct observation of cyclic carbenium ions and their role in the catalytic cycle of the methanol-to-olefin reaction over chabazite zeolites. *Angew. Chem. Int. Ed.* **52**, 11564–11568 (2013).
54. Song, W., Nicholas, J. B., Sassi, A. & Haw, J. F. Synthesis of the heptamethylbenzenium cation in zeolite: *in situ* NMR and theory. *Catal. Lett* **81**, 49–53 (2002).
55. Bollini, P. & Bhan, A. Improving HSAPO-34 methanol-to-olefin turnover capacity by seeding the hydrocarbon pool. *ChemPhysChem* **19**, 479–483 (2018).
56. Martinez-Espin, J. S. et al. New insights into catalyst deactivation and product distribution of zeolites in the methanol-to-hydrocarbons (MTH) reaction with methanol and dimethyl ether feeds. *Catal. Sci. Technol* **7**, 2700–2716 (2017).
57. Muller, S. et al. Coke formation and deactivation pathways on H-ZSM-5 in the conversion of methanol to olefins. *J. Catal.* **325**, 48–59 (2015).
58. Hwang, A. & Bhan, A. Bifunctional strategy coupling Y_2O_3-catalyzed alkanal decomposition with methanol-to-olefins catalysis for enhanced lifetime. *ACS Catal* **7**, 4417–4422 (2017).

59. Yarulina, I., Kapteijn, F. & Gascon, J. The importance of heat effects in the methanol to hydrocarbons reaction over ZSM-5: on the role of mesoporosity on catalyst performance. *Catal. Sci. Technol* **6**, 5320–5325 (2016).
60. Mole, T., Whiteside, J. A. & Seddon, D. Aromatic co-catalysis of methanol conversion over zeolite catalysts. *J. Catal.* **82**, 261–266 (1983).
61. Wu, W. Z., Guo, W. Y., Xiao, W. D. & Luo, M. Dominant reaction pathway for methanol conversion to propene over high silicon H-ZSM-5. *Chem. Eng. Sci.* **66**, 4722–4732 (2011).
62. Ilias, S., Khare, R., Malek, A. & Bhan, A. A descriptor for the relative propagation of the aromatic- and olefin-based cycles in methanol-to-hydrocarbons conversion on H-ZSM-5. *J. Catal.* **303**, 135–140 (2013).
63. Ilias, S. & Bhan, A. Tuning the selectivity of methanol-to-hydrocarbons conversion on H-ZSM-5 by co-processing olefin or aromatic compounds. *J. Catal.* **290**, 186–192 (2012).
64. Khare, R. & Bhan, A. Mechanistic studies of methanol-to-hydrocarbons conversion on diffusion-free MFI samples. *J. Catal.* **329**, 218–228 (2015).
65. Ito, H. et al. Method for production of lower olefin. European patent EP1955989 A1 (2008).
66. Chikamatsu, N., Funatsu, S., Ito, H., Oyama, K. & Yoshida, J. Propylene production process and propylene production apparatus. EP2058290 A1; (2009).
67. Smit, B. & Maesen, T. L. M. Towards a molecular understanding of shape selectivity. *Nature* **451**, 671–678 (2008).
68. Hereijgers, B. P. C. et al. Product shape selectivity dominates the methanol-to-olefins (MTO) reaction over H-SAPO-34 catalysts. *J. Catal.* **264**, 77–87 (2009).
69. Chen, D., Moljord, K., Fuglerud, T. & Holmen, A. The effect of crystal size of SAPO-34 on the selectivity and deactivation of the MTO reaction. *Microporous Mesoporous Mater* **29**, 191–203 (1999).
70. Moliner, M., Martínez, C. & Corma, A. Synthesis strategies for preparing useful small pore zeolites and zeotypes for gas separations and catalysis. *Chem. Mater.* **26**, 246–258 (2014).
71. Zhong, J. et al. Increasing the selectivity to ethylene in the MTO reaction by enhancing diffusion limitation in the shell layer of SAPO-34 catalyst. *Chem. Commun.* **54**, 3146–3149 (2018).
72. Li, J. et al. Cavity controls the selectivity: insights of confinement effects on MTO reaction. *ACS Catal* **5**, 661–665 (2015).
73. Yarulina, I. et al. Methanol-to-olefins process over zeolite catalysts with DDR topology: effect of composition and structural defects on catalytic performance. *Catal. Sci. Technol* **6**, 2663–2678 (2016).
74. Chen, D., Moljord, K. & Holmen, A. A methanol to olefins review: diffusion, coke formation and deactivation SAPO type catalysts. *Microporous Mesoporous Mater* **164**, 239–250 (2012).
75. Haw, J. F., Song, W. G., Marcus, D. M. & Nicholas, J. B. The mechanism of methanol to hydrocarbon catalysis. *Acc. Chem. Res.* **36**, 317–326 (2003).
76. Chen, J. et al. Spatial confinement effects of cage-type SAPO molecular sieves on product distribution and coke formation in methanol-to-olefin reaction. *Catal. Commun.* **46**, 36–40 (2014).
77. Bhawe, Y. et al. Effect of cage size on the selective conversion of methanol to light olefins. *ACS Catal* **2**, 2490–2495 (2012).
78. Dusselier, M., Deimund, M. A., Schmidt, J. E. & Davis, M. E. Methanol-to-olefins catalysis with hydrothermally treated zeolite SSZ-39. *ACS Catal* **5**, 6078–6085 (2015).
79. Pinilla-Herrero, I., Olsbye, U., Márquez-Álvarez, C. & Sastre, E. Effect of framework topology of SAPO catalysts on selectivity and deactivation profile in the methanol-to-olefins reaction. *J. Catal.* **352**, 191–207 (2017).
80. Kang, J. H. et al. Further studies on how the nature of zeolite cavities that are bounded by small pores influences the conversion of methanol to light olefins. *ChemPhysChem* **19**, 412–419 (2018).
81. Liang, T. et al. Conversion of methanol to olefins over H-ZSM-5 zeolite: reaction pathway is related to the framework aluminum siting. *ACS Catal.* **6**, 7311–7325 (2016).
A comprehensive article showing the effect of aluminium siting and location on selectivtiy and lifetime.
82. Bleken, F. et al. Conversion of methanol over 10-ring zeolites with differing volumes at channel intersections: comparison of TNU-9, IM-5, ZSM-11 and ZSM-5. *Phys. Chem. Chem. Phys.* **13**, 2539–2549 (2011).
83. Cui, Z.-M., Liu, Q., Song, W.-G. & Wan, L.-J. Insights into the mechanism of methanol-to-olefin conversion at zeolites with systematically selected framework structures. *Angew. Chem. Int. Ed.* **45**, 6512–6515 (2006).
84. Teketel, S., Svelle, S., Lillerud, K.-P. & Olsbye, U. Shape-selective conversion of methanol to hydrocarbons over 10-ring unidirectional-channel acidic H-ZSM-22. *ChemCatChem* **1**, 78–81 (2009).
85. Teketel, S. et al. Shape selectivity in the conversion of methanol to hydrocarbons: the catalytic performance of one-dimensional 10-ring zeolites: ZSM-22, ZSM-23, ZSM-48, and EU-1. *ACS Catal.* **2**, 26–37 (2012).
This article discusses how slight changes in pore dimensions profoundly affect selectivity to hydrocarbons establishing topology as a tool to control selectivity.
86. Jamil, A. K. et al. Selective production of propylene from methanol conversion over nanosized ZSM-22 zeolites. *Ind. Eng. Chem. Res.* **53**, 19498–19505 (2014).
87. Molino, A. et al. Conversion of methanol to hydrocarbons over zeolite ZSM-23 (MTT): exceptional effects of particle size on catalyst lifetime. *Chem. Commun.* **53**, 6816–6819 (2017).
88. Ma, H. et al. Reaction mechanism for the conversion of methanol to olefins over H-ITQ-13 zeolite: a density functional theory study. *Catal. Sci. Technol* **8**, 521–533 (2018).
89. Westgård Erichsen, M., Svelle, S. & Olsbye, U. The influence of catalyst acid strength on the methanol to hydrocarbons (MTH) reaction. *Catal. Today* **215**, 216–223 (2013).
90. Mikkelsen, Ø. & Kolboe, S. The conversion of methanol to hydrocarbons over zeolite H-beta. *Microporous Mesoporous Mater* **29**, 173–184 (1999).
91. Abubakar, S. M. et al. Structural and mechanistic investigation of a phosphate-modified HZSM-5 catalyst for methanol conversion. *Langmuir* **22**, 4846–4852 (2006).
92. Liu, J. et al. Methanol to propylene: effect of phosphorus on a high silica HZSM-5 catalyst. *Catal. Commun.* **10**, 1506–1509 (2009).
93. Hu, S. et al. Selective formation of propylene from methanol over high-silica nanosheets of MFI zeolite. *Appl. Catal. A* **445**, 215–220 (2012).
94. Mei, C. et al. Selective production of propylene from methanol: mesoporosity development in high silica HZSM-5. *J. Catal.* **258**, 243–249 (2008).
95. Wen, M. et al. Monolithic metal-fiber@HZSM-5 core–shell catalysts for methanol-to-propylene. *Microporous Mesoporous Mater* **206**, 8–16 (2015).
96. Wei, R., Li, C., Yang, C. & Shan, H. Effects of ammonium exchange and Si/Al ratio on the conversion of methanol to propylene over a novel and large partical size ZSM-5. *J. Nat. Gas Chem.* **20**, 261–265 (2011).
97. Khare, R., Liu, Z., Han, Y. & Bhan, A. A mechanistic basis for the effect of aluminum content on ethene selectivity in methanol-to-hydrocarbons conversion on HZSM-5. *J. Catal.* **348**, 300–305 (2017).
98. Yarulina, I. et al. Suppression of the aromatic cycle in methanol-to-olefins reaction over ZSM-5 by post-synthetic modification using calcium. *ChemCatChem* **8**, 3057–3063 (2016).
99. van der Bij, H. E. & Weckhuysen, B. M. Phosphorus promotion and poisoning in zeolite-based materials: synthesis, characterisation and catalysis. *Chem. Soc. Rev.* **44**, 7406–7428 (2015).
100. Danilina, N., Krumeich, F., Castelanelli, S. A. & van Bokhoven, J. A. Where are the active sites in zeolites? Origin of aluminum zoning in ZSM-5. *J. Phys. Chem. C* **114**, 6640–6645 (2010).
101. von Ballmoos, R. & Meier, W. M. Zoned aluminium distribution in synthetic zeolite ZSM-5. *Nature* **289**, 782 (1981).
102. Althoff, R., Schulzdobrick, B., Schüth, F. & Unger, K. Controlling the spatial distribution of aluminum in ZSM-5 crystals. *Microporous Mater.* **1**, 207–218 (1993).
103. Roeffaers, M. B. J. et al. Space- and time-resolved visualization of acid catalysis in ZSM-5 crystals by fluorescence microscopy. *Angew. Chem. Int. Ed.* **46**, 1706–1709 (2007).
104. Kox, M. H. F., Stavitski, E. & Weckhuysen, B. M. Nonuniform catalytic behavior of zeolite crystals as revealed by *in situ* optical microspectroscopy. *Angew. Chem. Int. Ed.* **46**, 3652–3655 (2007).
105. Tzoulaki, D., Heinke, L., Schmidt, W., Wilczok, U. & Kärger, J. Exploring crystal morphology of nanoporous hosts from time-dependent guest profiles. *Angew. Chem. Int. Ed.* **47**, 3954–3957 (2008).
106. Mores, D. et al. Space- and time-resolved *in-situ* spectroscopy on the coke formation in molecular sieves: methanol-to-olefin conversion over H-ZSM-5 and H-SAPO-34. *Chem. Eur. J* **14**, 11320–11327 (2008).
107. Mores, D., Kornatowski, J., Olsbye, U. & Weckhuysen, B. M. Coke formation during the methanol-to-olefin conversion: in situ microspectroscopy on individual H-ZSM-5 crystals with different brønsted acidity. *Chem. Eur. J* **17**, 2874–2884 (2011).
108. Perea, D. E. et al. Determining the location and nearest neighbours of aluminium in zeolites with atom probe tomography. *Nat. Commun.* **6**, 7589 (2015).
109. Schmidt, J. E. et al. coke formation in a zeolite crystal during the methanol-to-hydrocarbons reaction as studied with atom probe tomography. *Angew. Chem. Int. Ed.* **55**, 11173–11177 (2016).
In this article, atom probe tomography was used to spatially resolve the 3D compositional changes at the sub-nm length scale in a partially deactivated single zeolite ZSM-5 crystal after the methanol-to-hydrocarbon reaction.
110. Bleken, F. et al. The effect of acid strength on the conversion of methanol to olefins over acidic microporous Catalysts with the CHA topology. *Top. Catal* **52**, 218–228 (2009).
111. Westgård Erichsen, M. et al. How zeolitic acid strength and composition alter the reactivity of alkenes and aromatics towards methanol. *J. Catal.* **328**, 186–196 (2015).
112. Goetze, J. et al. Insights into the activity and deactivation of the methanol-to-olefins process over different small-pore zeolites as studied with operando UV–vis spectroscopy. *ACS Catal* **7**, 4033–4046 (2017).

113. Goetze, J., Yarulina, I., Gascon, J., Kapteijn, F. & Weckhuysen, B. M. Revealing lattice expansion of small-pore zeolite catalysts during the methanol-to-olefins process using combined *operando* X-ray diffraction and UV–vis spectroscopy. *ACS Catal* **8**, 2060–2070 (2018).
114. Chowdhury, A. D. et al. Electrophilic aromatic substitution over zeolites generates Wheland-type reaction intermediates. *Nat. Catal* **1**, 23–31 (2018).
115. Vogt, C., Weckhuysen, B. M. & Ruiz-Martínez, J. Effect of feedstock and catalyst impurities on the methanol-to-olefin reaction over H-SAPO-34. *ChemCatChem* **9**, 183–194 (2017).
116. Gao, P. et al. Direct conversion of CO_2 into liquid fuels with high selectivity over a bifunctional catalyst. *Nat. Chem* **9**, 1019 (2017).
117. Jiao, F. et al. Selective conversion of syngas to light olefins. *Science* **351**, 1065–1068 (2016).

Competing interests
The authors declare no competing interests.

Additional information
Supplementary information is available for this paper at https://doi.org/10.1038/s41929-018-0078-5.

Reprints and permissions information is available at www.nature.com/reprints.

Correspondence should be addressed to B.M.W. or J.G.

Publisher's note: Springer Nature remains neutral with regard to jurisdictional claims in published maps and institutional affiliations.